Research in Astron. Astrophys. **2011** Vol. **11** No. **5**, 563–576
http://www.raa-journal.org *http://www.iop.org/journals/raa*

Research in Astronomy and Astrophysics

Metallicity calibration for solar type stars based on red spectra *

Jing-Kun Zhao, Gang Zhao, Yu-Qin Chen and A-Li Luo

Key Laboratory of Optical Astronomy, National Astronomical Observatories, Chinese Academy of Sciences, Beijing 100012, China; *gzhao@bao.ac.cn*

Received 2010 February 3; accepted 2010 December 14

Abstract Based on a high resolution and high signal-to-noise ratio (S/N) spectral analysis of 90 solar-type stars, we have established several new metallicity calibrations in the $T_{\rm eff}$ range [5600, 6500] K based on red spectra with the wavelength range of 560–880 nm. The new metallicity calibrations are applied to determine the metallicity of solar analogs selected from Sloan Digital Sky Survey (SDSS) spectra. There is a good consistent result with the adopted value presented in SDSS-DR7 and a small scatter of 0.26 dex for stars with S/N $>$ 50 being obtained. This study provides a new reliable way to derive the metallicity for solar-like stars with low resolution spectra. In particular, our calibrations are useful for finding metal-rich stars, which are missing in the SEGUE Stellar Parameter Pipeline.

Key words: techniques: radial velocities — stars: temperatures — stars: abundances

1 INTRODUCTION

The stellar spectroscopic survey with the Large Area sky Multi-Object fiber Spectroscopic Telescope (LAMOST), now named the Guoshoujing Telescope, will provide a huge amount of data, which can be used for the study of chemical and kinematical evolution of our Galaxy. In this respect, stellar metallicity and radial velocity, being two main parameters, can be derived from spectra. The determination of radial velocity is generally easier mainly by using either cross-correlation of the template spectra or Doppler shift through line calibration. The consistency is usually quite good depending on the quality of the spectra. The metallicity estimation from stellar spectra is based on various methods, as shown in Lee et al. (2008a) (hereafter Lee08). However, for solar type stars, these values can be underestimated by up to 0.5 dex in the previous version of the SEGUE Stellar Parameter Pipeline (SSPP) (Lee08). The current version of SSPP has made great improvements, reaching about 0.1 dex in the underestimation (Lee et al. 2008b). From figure A1 in Bond et al. (2010), the largest difference between the Sloan Digital Sky Survey (SDSS) (York et al. 2000) spectroscopic metallicity values from Data Release 6 (DR6) (Adelman-McCarthy et al. 2008) and those from Data Release 7 (DR7) (Abazajian et al. 2009) is shown for solar type stars, so it is worth the effort to do more research about deriving the metallicity of those stars.

In this work, we attempt to establish a new metallicity calibration for low resolution solar type stars based on the result from high resolution and high signal-to-noise ratio spectral analysis performed by Chen et al. (2000, hereafter Chen00). In comparison with the methods presented in Lee08, this work has some advantages. Firstly, the calibration is based on the real stellar (empirical) spectra and their metallicity is derived from the fine analysis of high resolution and high S/N spectra.

∗ Supported by the National Natural Science Foundation of China.

Secondly, we have used the red spectral coverage of 560–880 nm, but most of the methods in Lee08 are based on blue spectra with $\lambda < 600$ nm. As is well known, the advantage of the red spectra is that it is easier to define the continuum, which is not possible for blue spectra due to the heavy line blanketing at low resolution observations. In view of this advantage, we adopted the equivalent widths (EWs) of individual lines in the calibration instead of the line index. As for line index, there might be a different definition for different authors while the EW remains a fixed value. For example, in the CaII K line, there are K6, K12 and K18 among its possible definitions. If we can define the continuum well, the EW is better than the line index. Thirdly, we have adopted only Fe lines for metallicity calibration and avoided contributions from other elements, which do not exactly trace iron evolution at different times and different nucleosynthesis sites. In Lee08, the wavelength ranges of matching templates include all the separate lines from different elements. The KP spectral line index is also an indicator of [Ca/H]. Although these weak Fe lines are undetectable in metal-poor stars because of the noise, we can recognize them in solar type stars where the S/N is higher than 20. Moreover, the EW of weak lines is more sensitive to abundance than that of strong lines. For high resolution spectral analysis, strong lines, e.g. Na 5895Å and Na 5890Å, are saturated and in the growth curve the increasing EWs do not give higher abundance values. In general, the EW of strong lines does not change a lot with the degradation of resolution. In view of this, it is not an optimal strategy to establish a relation between abundance and EW in combination with colors using a very strong line. Finally, the calibration is internally consistent, but Lee08 adopted the average of different values from various methods.

In Section 2, a description of the data for the calibration is presented. The template matching analysis is described in Section 3. The detailed analysis procedure to get the calibration formula is given in Section 4. The application of the calibration to SDSS spectra is illustrated in Section 5. Finally, conclusions are given in Section 6.

2 DATA

The real spectra are taken from Chen00 which has a resolving power of 37 000 and S/N of 150–300 obtained with the Coud$\acute{e}$ Echelle Spectrograph mounted on the 2.16 m telescope of the National Astronomical Observatories (Zhao & Li 2001). The sample has $T_{\rm eff}$, $\log g$ and [Fe/H] distributions as shown in Figure 1. It is clear that $T_{\rm eff}$ ranges between [5600, 6500]K, $\log g$ is in [3.98, 4.43] and [Fe/H] is in [–1.04, 0.06]. Moreover, the range of $b-y$ is within [0.28, 0.43], $B-V$ is within [0.40, 0.67], $V-I$ is within [0.46, 0.73] and $V-K$ is within [0.9, 1.65]. We convolved the normalized spectra to a low resolution of 2000 with a Gaussian function. In addition, the spectra were rebinned to 1.5Å/pix after being smoothed to $R \sim$2000.

3 THE TEMPLATE MATCHING ANALYSIS

Following one method of Lee08, we perform the template spectral match (also see Allende Prieto et al. 2006, Re Fiorentin et al. 2007 and Zwitter et al. 2005) for the normalized low resolution spectra of 90 stars and derived the stellar temperature, gravity and metallicity. Using this method, we generate a library of low resolution theoretical spectra by using the SYNTH program based on the Kurucz New ODF (Castelli & Kurucz 2003) atmospheric models. The atmosphere models are derived under the assumption of local thermodynamic equilibrium (LTE). The mixing-length is adopted to be l/Hp = 1.25 and microturbulence is 1.5 km s^{-1}. The line list, including the atoms and molecules, are all from Kurucz (1993). The molecular species include CH, CN, OH, and TiO. Solar abundances are from Asplund (2005). As for those grids, $T_{\rm eff}$ covers the range [3500, 9750]K in intervals of 250 K; $\log g$ is within [1.0, 5.0] dex in intervals of 0.5 dex; [Fe/H] is within [–4.0, –3.0] dex in intervals of 0.25 dex and intervals of 0.1 dex in the range [–3.0, +0.5] dex. The minimum distance method is applied to obtain the parameters by interpolation among several of the closest theoretical spectra to the observed one.

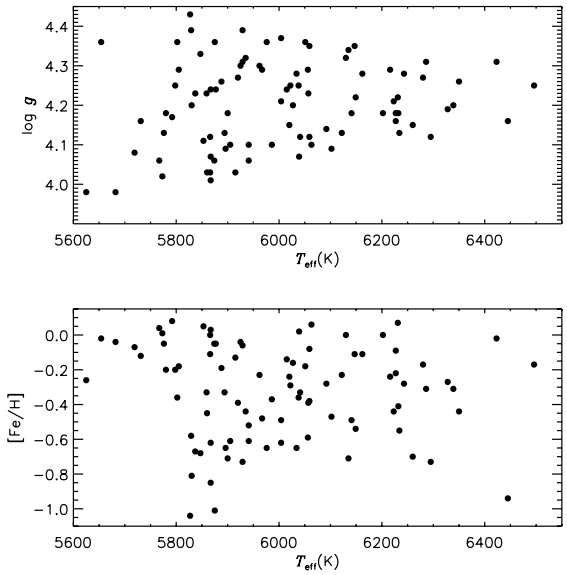

Fig. 1 Stellar parameter distribution of the sample in Chen00.

Table 1 [Fe/H] Results of Template Matching with Different Wavelength Ranges

Wavelength range (nm)	Mean deviation	Scatter
570–653	0.448	0.175
570–684	0.226	0.275
570–700	0.016	0.230
640–670	0.470	0.280
651–662	0.599	0.390
690–713	–0.07	0.590
735–756	0.350	0.290
772–810	–0.100	0.260

We have adopted different wavelength ranges in the matching procedure and obtained different results as shown in Table 1. As compared with the 'standard' values presented in the Chen00 paper, we have found that the spectral range of 570–700 nm is the best choice with a mean deviation of 0.016 dex and scatter of 0.23 dex in [Fe/H]. The comparison of temperature and metallicity of the 570–700 nm spectral range is shown in Figure 2. It is clear that the temperature estimation has a systematical deviation toward a lower value in the present work. Since the high resolution spectra in Chen00 are obtained with the Echelle spectrograph, the order is not wide enough to include the whole Hα line region and the normalization is implemented order by order. Thus, the continuum is not very reliable in the Hα region, which might be the reason for the systematical deviation in temperature estimation. The metallicity is quite consistent with an rms of 0.23 dex.

4 [FE/H] vs. EW OF THE Fe I LINE – AN EMPIRICAL CALIBRATION

Although the template matching method can be used to obtain accurate stellar parameters, it may give different results with different wavelength ranges. Hence, we will determine stellar metallicity based on the strength of some Fe I lines.

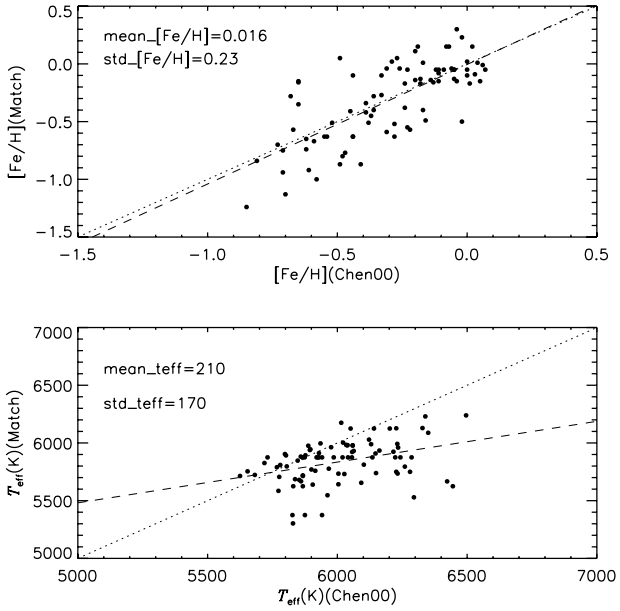

Fig. 2 [Fe/H] and $T_{\rm eff}$ comparison between those of Chen00 and the results from the template matching with a spectral range of 570 nm–750 nm.

4.1 The Selection of Spectral Lines

What we want is to choose some Fe lines that are not heavily blended and have better profiles in the low resolution (R ∼2000) spectra. At the beginning, we draw the original spectrum, then overplot the low resolution spectrum on it. After checking the lines one by one, we select five Fe I lines as our indices of metallicity. The spectral lines for three stars with different metallicity values are given in Figure 3: HD94280 has [Fe/H] of 0.06; HD100446 has –0.48; HD184601 has –0.81. In Figure 3, the solid line is the high resolution spectrum while the thick dotted line is that of the low resolution one. In this segment of the spectrum, only two Fe I lines meet our requirements since they are detectable; they have good shapes and are not seriously blended in the spectra with a resolution of R ∼2000. From the top to the bottom of Figure 3, it is obvious that the strength of the Fe I lines decreases. Also, for stars with [Fe/H] > -0.8, the two lines can be identified.

Table 2 Definition of Fe I Lines

Left	Right	Center
6060.917	6069.954	6065.492
6217.769	6221.788	6219.292
6391.147	6395.953	6393.605
6398.256	6402.209	6400.232
6675.000	6682.326	6678.256

Table 2 presents the definition of five Fe I line indices used for our metallicity calibration. There are three parts for each line including red, center and blue components. The EW of each line can be measured by using a direct integration method.

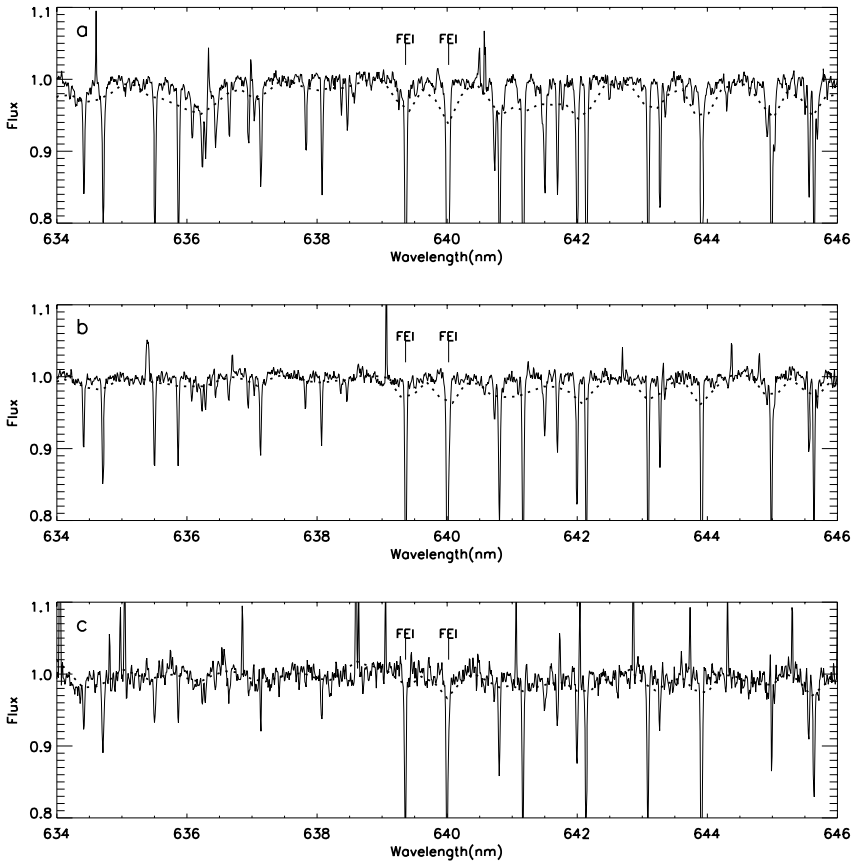

Fig. 3 A portion of the spectra: (a) HD94280 ($T_{\rm eff}$ = 6063 K, $\log g$ = 4.10, [Fe/H]= 0.06); (b) HD100446 ($T_{\rm eff}$ = 5967 K, $\log g$ = 4.29, [Fe/H]= −0.48); (c) HD184601 ($T_{\rm eff}$ = 5830 K, $\log g$ = 4.20, [Fe/H]= −0.81). The solid lines are the high resolution spectra while the thick dotted lines are the low resolution spectra. The two Fe I lines are those that meet the stated requirements.

4.2 The Metallicity Calibration Based on EWs

Since our spectra are normalized and there are no spectra with flux calibration, it is difficult to derive reliable temperature measurements. In order to improve the metallicity determination, we resort to using the strengths of iron lines and establish a calibration between metallicity and EWs of iron lines. The EWs are derived with Equation (1).

$$\mathrm{EW} = \int_{\lambda 1}^{\lambda 2} \frac{f_{\rm c} - f_\lambda}{f_{\rm c}} d_\lambda \tag{1}$$

In Equation (1), the f_λ represents the flux of wavelength λ, while $f_{\rm c}$ means the continuum of wavelength λ. It is shown in Figure 4 that there is a good correlation between [Fe/H] and EWs for the five Fe I lines for stars whose [Fe/H] $>$ –0.8. The calibration (Eq. (2)) for each line is shown in Table 3.

$$[\mathrm{Fe/H}] = a + b \times \mathrm{EW(Fe\,I)}\,. \tag{2}$$

Table 3 Coefficients and σ values of the fitting between [Fe/H] and EW for each Fe I line.

Line	a	b	σ
Fe I1	–0.922	5.063	0.170
Fe I2	–0.866	6.559	0.143
Fe I3	–1.010	5.960	0.167
Fe I4	–0.970	4.958	0.163
Fe I5	–1.026	6.056	0.204

Table 4 Coefficients and σ values of [Fe/H] calibration based on the EW of five Fe I lines and temperature.

Line	a	b	c	σ
Fe I1	1.731	5.929	–3.281	0.150
Fe I2	2.138	7.726	–3.692	0.112
Fe I3	2.282	7.386	–4.116	0.136
Fe I4	2.793	6.381	–4.702	0.122
Fe I5	0.974	6.949	–2.505	0.194

As seen in Figure 4, Fe I2 and Fe I4 show the best result with the lowest scatter in the relation. To show the temperature effect of EW, we divide the temperature range into three parts. The first part is the range [5265, 5900], the second part is [5900, 6200] and the last part is [6200, 6496]. In Figure 5, the stars in the first part are given with the symbol of the dot and asterisks represent the stars in the second part, while the stars in the last part are plotted with diamonds. From Figure 5, it is clear that the relation between EW and [Fe/H] changes with temperature. Fe I2 and Fe I4 have lower scatter than other Fe I lines and this may be due to the lower sensitivity of line strength with temperature. In order to understand this issue, we added the temperature term in the calibration of Figure 6. The coefficients and scatter of each line are given in Table 4. It is obvious that the σ value becomes small for the calibration of each line after considering the effect of temperature. Since the temperature is usually unknown in the spectral analysis, it may be good to replace the temperature term with the color index. Thus, we collected $(b-y)$, $(B-V)$, $(V-I)$ and $(V-K)$ and performed a similar calibration (Eq. (3)). Also, $\log g$ will cause more or less uncertainty in the metallicity determination. However, the gravity range considered in the calibration sample is narrow, hence its effect is very little and could be ignored.

Table 5 is the coefficients and scatter of the calibration of [Fe/H] through EW and $B-V$.

$$[\mathrm{Fe/H}] \;=\; a + b \times \mathrm{EW(Fe\,I)} + c \times (B-V)\,. \tag{3}$$

Table 5 Coefficients, σ values and the EW ranges of the fitting between [Fe/H] and the EW plus $B-V$ for each Fe I line.

Line	a	b	c	σ	EW range
Fe I1	–0.790	5.351	–0.315	0.169	0.025∼0.225
Fe I2	–0.290	8.144	–1.342	0.132	0.006∼0.158
Fe I3	–0.555	7.352	–1.167	0.160	0.044∼0.185
Fe I4	–0.321	6.622	–1.643	0.151	0.029∼0.224
Fe I5	–1.200	5.497	0.453	0.202	0.046∼0.193

4.3 Calibration in the Miles Spectral Library

To make an external calibration, we selected 107 spectra from the Miles spectral library (Sánchez-Blázquez et al. 2006; Cenarro et al. 2007) which meet the following conditions: –0.8 $\leq$ [Fe/H] $\leq$ 0.5; 4.0 $\leq \log g \leq$4.5; 5600 $\leq T_{\rm eff} \leq$ 6500. Thus, it is possible to estimate the metallicity of these 107 spectra using the above calibrations. The resolution of the Miles spectra is about 2.3Å and the wavelength has already been calibrated with radial velocity. First, we do normalization for these 107 spectra. The continuum is determined by iterative smoothing with a Gaussian profile, and then clipping off points that lie beyond 1 σ or 4 σ above the smoothed curve. Second, the EWs of five Fe I lines are measured. $B-V$ of those 107 stars are taken from the literature identified in the Simbad

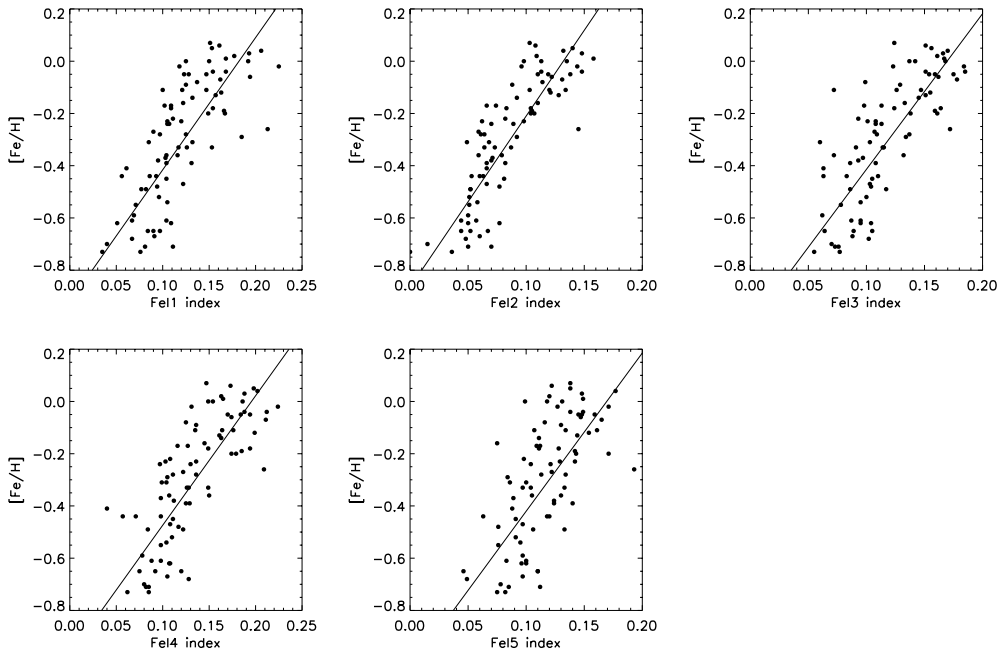

Fig. 4 Relation between [Fe/H] and EW for five Fe I lines for the stars with [Fe/H] > -0.8.

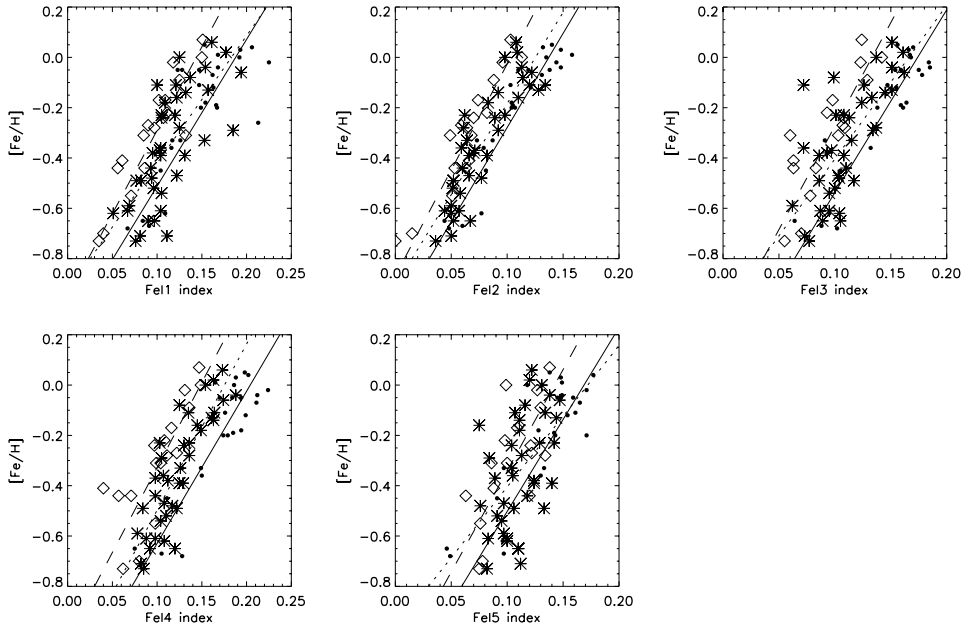

Fig. 5 Relation between the metallicity and EW of Fe I lines in different $T_{\rm eff}$ ranges. Dots represent stars in [5265, 5900] K; asterisks are those in [5900, 6200] K; diamonds are those in [6200, 6500] K.

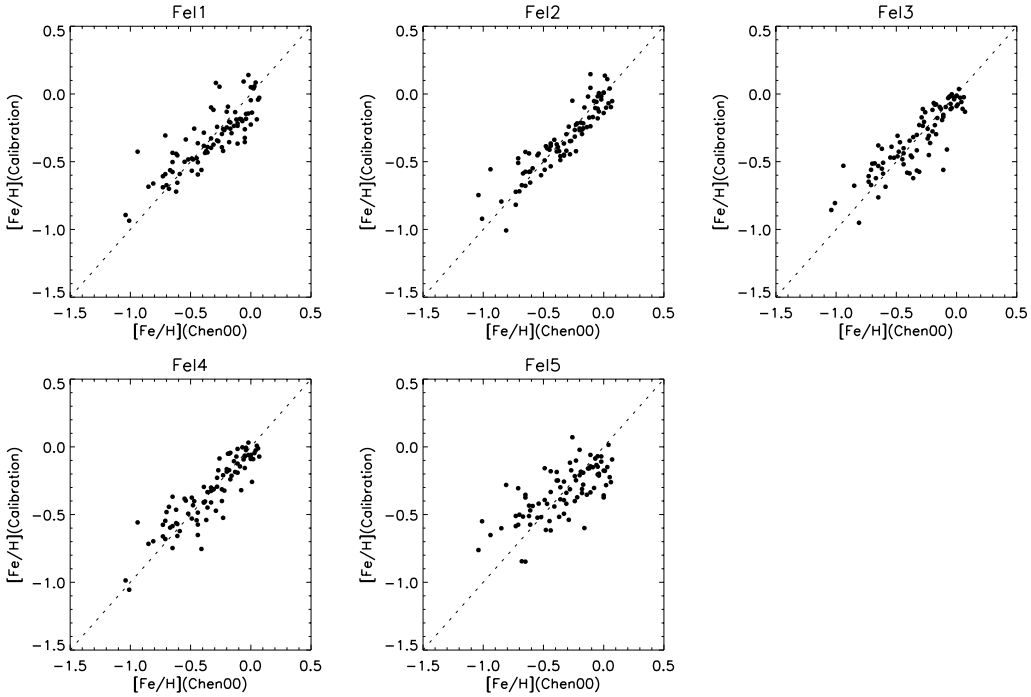

Fig. 6 Comparison between [Fe/H] in Chen00 and that of the calibration from each Fe I line and the temperature.

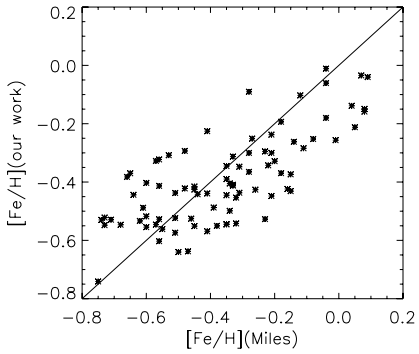

Fig. 7 Application of our [Fe/H] calibration in Miles' spectral library. The x axis is [Fe/H] from the Miles catalog and the y axis is [Fe/H] obtained by our calibration. The solid line is $x = y$.

Astronomical Database (Genova 2006). Finally, the metallicities are derived by the EW of the Fe I4 line using Equation (3) (the coefficients are shown in Table 5).

Figure 7 is the comparison of [Fe/H] between our results and those from the Miles library. The mean error is about 0.08 dex, and the scatter is about 0.21 dex. [Fe/H] of the Miles library is obtained by the compilation from the literature. This suggests that our metallicity is basically consistent with that of other work.

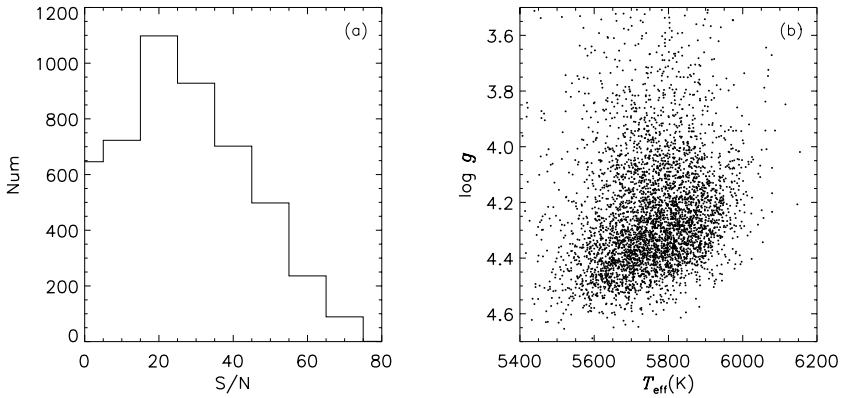

Fig. 8 Plots of (a) number vs. S/N (b) $\log g$ vs. $T_{\rm eff}$.

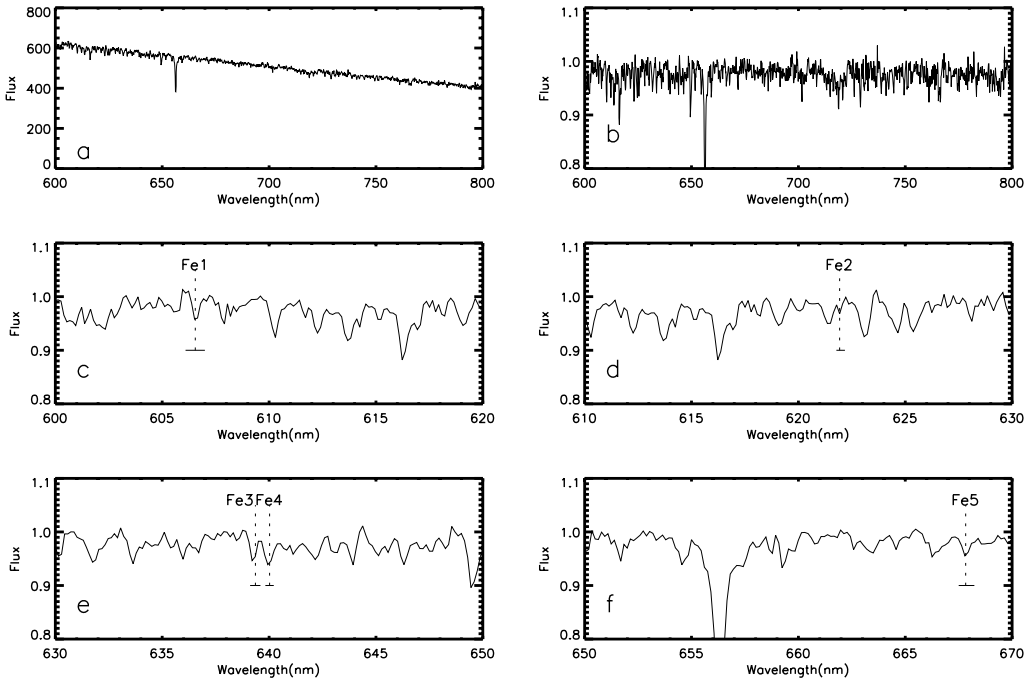

Fig. 9 Spectra of 53738–2051–030. Here 'a' is the original spectrum while 'b' is the normalized spectrum ($T_{\rm eff} = 5640$ K, $\log g = 4.49$, [Fe/H]$= -0.54$). Also, 'c,' 'd,' 'e,' 'f' and 'g' represent the spectral lines in our calibration.

5 APPLICATION OF THESE CALIBRATIONS

In order to check the accuracy of the [Fe/H] calibration from the EW of five Fe I lines, we implement this calibration to determine [Fe/H] for solar-like stars with SDSS spectra. The selection limitation

is as follows: $0.4 < (g-r)_0 < 0.5$, $0.10 < (r-i)_0 < 0.14$, $0.02 < (i-z)_0 < 0.06$, and $g_0 < 20$. The above color ranges come from the color of the Sun and its related error bars. Based on this limitation, 4 356 stars are extracted from the SDSS DR7 archive.

Figure 8 presents the information of this sample, from which we can see that the peak of the S/N is 20; the effective temperature of most stars is located in the range [5500, 6000] K; $\log\ g$ is in [4.0, 4.5]. By transforming the equation of Bilir et al. (2005), the $g-r$ range of Chen00 is [0.197, 0.501], so it is possible to estimate the metallicity of these solar-like stars using Equations (2) and (3).

5.1 Preprocessing

Our first preprocessing procedures mainly include radial velocity correction and normalization. The value of radial velocity comes from the FIT head of each spectrum. The pseudocontinuum is determined with the same method illustrated in Section 4.3. Although the method of pseudocontinuum determination is different from that in Chen00, it is good enough for solar type stars in the red spectral region. Since the SDSS spectra are calibrated with relative flux, the pseudocontinuum in the red region is more easily represented by a lower order polynomial. Thus, iterative smoothing of the original spectrum with a Gaussian profile will yield a good continuum shape. After normalization, the EW of the lines can be measured by the direct integration method.

Figure 9 is an example of the SDSS spectrum. Here 'a' is the original spectrum while 'b' is the normalized spectrum. Also, 'c,' 'd,' 'e' and 'f' represent the Fe I lines in our calibration. It is clear that these Fe I lines are detectable and show a good profile in the SDSS spectra.

5.2 Calibration

After obtaining the EW of five Fe I lines, [Fe/H] can be determined by our calibration formula. We make some comparison between [Fe/H] from our calibration and those from SSPP. Equation (4) is the calibration formula based on the Fe I4 line. $B-V$ can be obtained from the $g-r$ transformation (Bilir et al. 2005).

Figure 10 is the [Fe/H] comparison between those from SSPP and the results from Equation (4). The comparison of stars with S/N $>$ 50 is shown in the top panel and the difference distribution is given in the bottom panel. It is clear that our calibration from Equation (4) is very consistent with [Fe/H] from SSPP for those cases with S/N $>$ 50. The mean difference is about 0.018 dex and the scatter is around 0.26 dex.

$$[\mathrm{Fe/H}] = -0.321 + 6.622 \times \mathrm{EW(Fe\,I4)} - 1.643 \times (B-V)\,. \quad (4)$$

Moreover, we extract 51 stars which meet these conditions: [Fe/H]$\geq$0 from our result; [Fe/H]$<$ 0 from SSPP; S/N$>$ 50. Hence, these 51 stars are metal rich stars if our result is right. For these 51 stars, the temperature range is about [5650, 5865] K and the gravity range is in [4.3, 4.5] dex. To check the reliability of our result, we make a comparison between the strength of some spectral lines in these stars and those in the Sun since $T_{\rm eff}$ and $\log\ g$ of these stars are very close to those of the Sun. If the strength is stronger than that of the Sun then this star can be regarded as a metal rich star and its [Fe/H] is larger than 0. Since the NaI and CaII lines are strong in the red band, these lines, as well as two Fe I lines, are selected for comparison. There are three cases: one is that the strengths of these lines are all stronger than those of the Sun (see Fig. 11); one is that the strengths of these lines are all close to those of the Sun (see Fig. 12); the others are taken as the third case (see Fig. 13). After comparison, there are 33 stars in the first case, 10 stars in the second case and 8 stars in the third case. In view of this, the metal rich stars account for 84% of these 51 stars. So our calibration also provides a reliable way to identify metal rich stars.

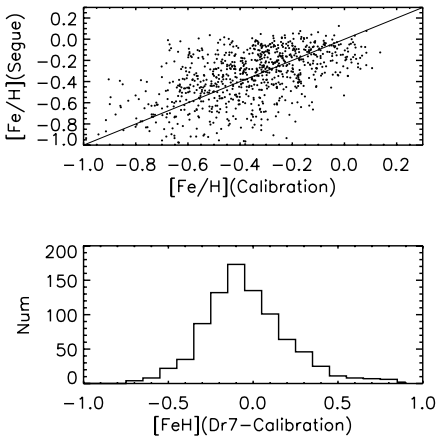

Fig. 10 [Fe/H] comparison of the SDSS solar-like stars between those from SSPP and those derived from the calibration using five Fe I lines.

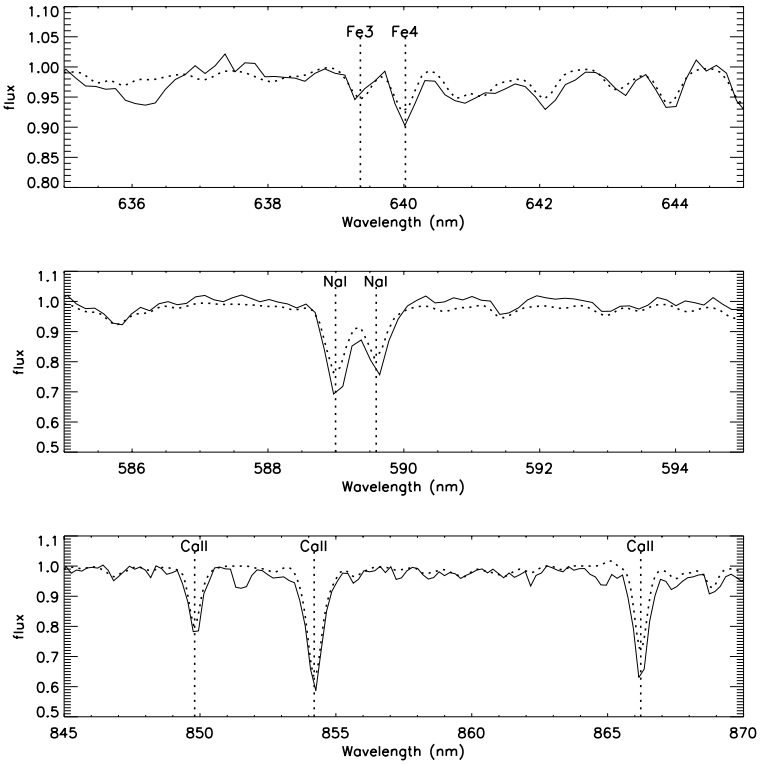

Fig. 11 Comparison of the strength of spectral lines. The solid lines are the object spectrum and the dotted lines are the solar spectrum. This is the case where the strengths of object lines are all stronger than those of the Sun.

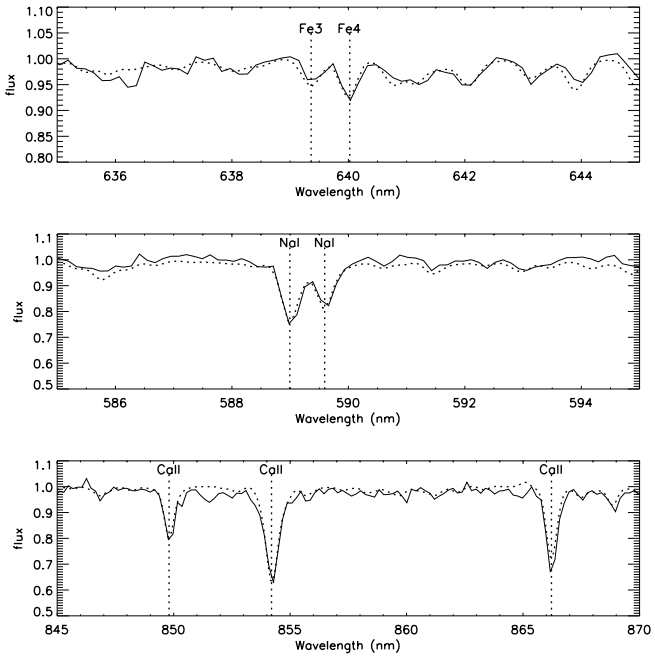

Fig. 12 Same as Fig. 11, but for the case where the strengths of object lines are all close to those of the Sun.

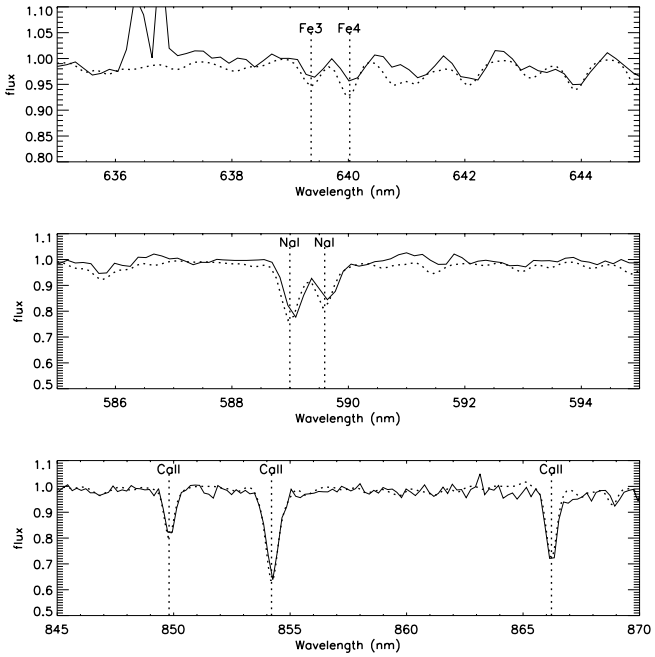

Fig. 13 Same as Fig. 11, but for the third case which includes others except the cases in Fig. 11 and Fig. 12.

5.3 The Effect of S/N

To investigate the S/N effect on our calibration, we selected seven spectra from DR7 with S/N (r band) $\sim$ 100. By introducing Gaussian noise in these spectra, we degraded them to S/N values of 50, 30, and 20. Then, normalization and EW measurements were carried out on all spectra. Finally, the metallicity values were derived with our above calibration. The left panel of Figure 14 presents the S/N effect on the metallicity change. Filled squares represent [Fe/H] changes for these seven stars with different S/N. Asterisks represent the average [Fe/H] changes for the given S/N. It can be seen that [Fe/H] changes about 0.22 dex from S/N = 100 to 20. [Fe/H] differences between our calibration results and those of SSPP vs. S/N are shown in the right panel of Figure 14. Asterisks are average differences and vertical lines represent scatters for the given S/N for these seven stars. Average [Fe/H] differences nearly remain the same but the scatter will be smaller than 0.4 dex when S/N is higher than 30. To sum up, our metallicity determination is quite robust to reductions in S/N.

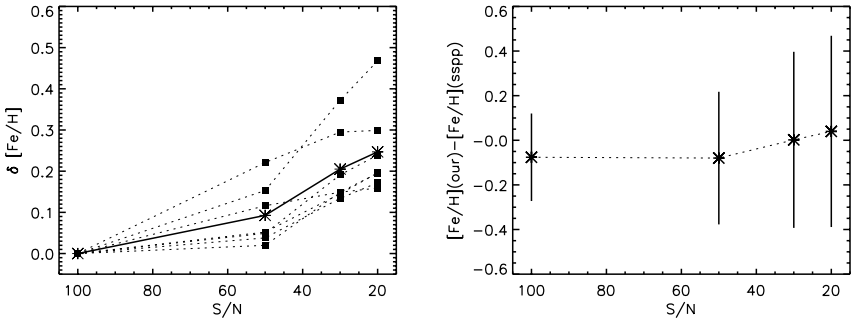

Fig. 14 *Left*: [Fe/H] change vs. S/N for seven stars. The original spectra of these seven stars were extracted from DR7 with S/N ∼100. By introducing Gaussian noise in the original spectra, we degraded them to S/N values of 50, 30, and 20. Filled squares are [Fe/H] changes of these seven stars with different S/N, while asterisks represent the average [Fe/H] change for the given S/N. *Right*: [Fe/H] differences between our calibration results and those from SSPP vs. S/N. Asterisks represent average [Fe/H] differences and vertical lines represent the scatter of the [Fe/H] differences at the given S/N.

6 CONCLUSIONS

For solar type stars, although template matching can derive reliable results with a suitable wavelength range, it is very difficult to determine the most appropriate wavelength range for matching.

We selected five Fe I lines from the red part of the R ∼2000 resolution spectra. These lines, which have a good profile, are not seriously blended and could be detectable with [Fe/H] > -0.8. At the beginning, the metallicity calibrations are set up only through the EW and the scatters are from 0.14 to 0.20 dex. The dispersion becomes small after adding the temperature into the calibrations. Since the temperature is usually unknown in the spectral analysis, it may be good to replace the temperature term with the color index. In view of this, several metallicity calibrations are constructed by the EW of Fe I lines and colors based on the 90 solar type stars. The dispersion of all the calibrations is smaller than 0.21 dex. Among the five Fe I lines, Fe I2 and Fe I4 have contributed the best calibrations (Eqs. (5) and (6)) which have the smallest scatters (0.13 dex and 0.15 dex).

$$[\mathrm{Fe/H}] = -0.290 + 8.144 \times \mathrm{EW(Fe\,I2)} - 1.342 \times (B - V), \quad 0.006 < \mathrm{EW(Fe\,I2)} < 0.158, \quad (5)$$

$$[\mathrm{Fe/H}] = -0.321 + 6.622 \times \mathrm{EW(Fe\,I4)} - 1.643 \times (B-V), \quad 0.029 < \mathrm{EW(Fe\,I4)} < 0.224. \quad (6)$$

Moreover, we use the calibration from the EW of Fe I4 and the $B-V$ to estimate [Fe/H] of the solar type stars in DR7. After comparing with the value from SSPP, our method gives a good consistency for S/N larger than 50. In addition, we analyze the stars for which [Fe/H] ≥ 0 by the spectral lines comparison and found that 84% of them are reliable. Usually, [Na/Fe]=0 and [Ca/Fe]=0 for stars with [Fe/H] $>$ –0.4 in the solar neighborhood. In view of this, Na and Ca lines are stronger in Fe-rich stars. So this provides a new formula to estimate [Fe/H] with the red band and presents a reliable way to identify metal rich stars.

Acknowledgements This work is supported by the National Natural Science Foundation of China under grant Nos. 10673015, 10821061, 10973021, 11078019 and 11073026, the National Basic Research Program of China (973 program) No. 2007CB815103/815403, the Academy program No. 2006AA01A120 and the Youth Foundation of the National Astronomical Observatories of China. Many thanks to James Wicker for his help in revising English grammar in this paper.

References

Abazajian, K. N., et al. 2009, ApJS, 182, 543
Adelman-McCarthy, J. K., et al. 2008, ApJS, 175, 297
Allende Prieto, C., Beers, T. C., Wilhelm, R., Newberg, H. J., Rockosi, C. M., Yanny, B., & Lee, Y. S. 2006, ApJ, 636, 804
Asplund, M. 2005, ARA&A, 43, 481
Bilir, S., Karaali, S., & Tunçel, S. 2005, Astronomische Nachrichten, 326, 321
Bond, N. A., et al. 2010, ApJ, 716, 1
Castelli, F., & Kurucz, R. L. 2003, Modelling of Stellar Atmospheres (IAU Symp. 210), ed. N. Piskunov, W. W. Weiss, D. F. Gray (San Francisco, CA: ASP), 20P
Cenarro, A. J., et al. 2007, MNRAS, 374, 664
Chen, Y. Q., Nissen, P. E., Zhao, G., Zhang, H. W., & Benoni, T. 2000, A&AS, 141, 491 (Chen00)
Genova F. 2006, Centre de Donnes astronomiques de Strasbourg (*http://simbad.ustrasbg.fr*)
Lee, Y. S., et al. 2008a, AJ, 136, 2022 (Lee08)
Lee, Y. S., et al. 2008b, AJ, 136, 2050
Re Fiorentin, P., Bailer-Jones, C. A. L., Lee, Y. S., Beers, T. C., Sivarani, T., Wilhelm, R., Allende Prieto, C., & Norris, J. E. 2007, A&A, 467, 1373
Sánchez-Blázquez, P., et al. 2006, MNRAS, 371, 703
York, D. G., et al. 2000, AJ, 120, 1579
Zhao, G., & Li, H.-B. 2001, ChJAA (Chin. J. Astron. Astrophys.), 1, 555
Zwitter, T., Munari, U., & Siebert, A. 2005, in Proceedings of the Gaia Symposium, The Three-Dimensional Universe with Gaia (ESASP), 576, 623